PCCP

Structural, Electronic and Magnetic Properties of Ni Nanoparticles Supported on the TiC(001) Surface

Journal:	*Physical Chemistry Chemical Physics*
Manuscript ID	CP-ART-09-2020-004884.R1
Article Type:	Paper
Date Submitted by the Author:	22-Oct-2020
Complete List of Authors:	Lozano-Reis, Pablo; Universitat de Barcelona, Ciència de Materials i Química Física & IQTCUB Sayós, Ramón; Universitat de Barcelona, Quimica Fisica; Institut de Quimica Teorica i Computacional, Rodriguez, Jose; Brookhaven National Laboratory, Chemistry Department Illas, Francesc; Universitat de Barcelona, Departament de Ciència de Materials i Química Física

Structural, Electronic and Magnetic Properties of Ni Nanoparticles Supported on the TiC(001) Surface

Pablo Lozano-Reis,[1] Ramón Sayós,[1] José A. Rodriguez, [2] Francesc Illas[1]

1) Departament de Ciència de Materials i Química Física & Institut de Química Teòrica i Computacional (IQTCUB), Universitat de Barcelona, C. Martí i Franquès 1, 08028 Barcelona, Spain

2) Department of Chemistry, Brookhaven National Laboratory, Upton, New York, 11973-5000, U.S.A.

Metals supported on transition metal carbides are known to exhibit good catalytic activity and selectivity, which is interpreted in terms of electron polarization induced by the support. In the present work we go one step farther and investigate the effect that a titanium carbide (TiC) support has on the structural, electronic, and magnetic properties of a series of Ni nanoparticles of increasing size exhibiting a two- or three-dimensional morphology. The obtained results show that three-dimensional nanoparticles are more stable and easier to form than their homologous two-dimensional counterparts. Also, comparison to previous results indicate that, when used as support, transition metal carbides have a marked different chemical activity with respect to oxides. The analysis of the magnetic moment of the supported nanoparticles evidences a considerable quenching of the magnetic moment that affects mainly the Ni atoms in close contact with the TiC substrate indicating that these atoms are likely to be responsible for the catalytic activity reported for these systems. The analysis of the electronic structure reveals the existence of chemical interactions between the Ni nanoparticle and the TiC support, even if the net charge transfer between both systems is negligible.

Introduction

Heterogeneous catalysed processes play an essential role in the chemical industry as over 90 % of the chemical manufacturing processes of the world are based on this technology.[1] Catalysis is also at the heart of strategies aimed to mitigate the climate change emergency that calls for a switch from fossil fuels towards green energies.[2,3] Unfortunately, covering the global energetic demand through these new energy sources it still out of reach. Consequently, considerable attention is paid to the catalytic chemical conversion of greenhouse gases such as CO_2 and CH_4 to added-value chemicals of industrial interest, thus creating a cyclic energetic economy. Here new heterogeneously catalysed processes are necessary and they are currently the focus of considerable research endeavours.

The commonest industrial catalysts are constituted of small to medium size metallic nanoparticles, often from scarce precious elements, anchored on some type of support, usually on metal oxides, sulphides or zeolites.[1] Due to its relatively high activity and low cost compared to noble metals, Ni-based catalysts are extensively used for CO_2 hydrogenation reaction leading to CO, CH_4 or methanol.[4-9] Ni catalysts are also used in the steam and dry reforming of methane reaction.[10-15] These catalysts usually involve nickel nanoparticles supported over different metal oxides.[4-9,10-15] In principle, the role of the support goes to disperse the metallic nanoparticles and thus to increase the effective surface area. However, there is increasing evidence that the role of the support goes well beyond this simple picture. There is compelling evidence that the metal support interactions can be detrimental as in the so-called strong metal support interactions (SMSI) introduced by Tauster.[16-18] These were finally understood as capping of the metal nanoparticles by support islands as a result of prolonged exposure at high temperature thus leading to a concomitant decrease in the number of active sites. There is also evidence that the metal-support interactions can be beneficial as shown by Bruix et al.[19] for the water gas shift reaction (WGSR) on a model catalyst consisting of Pt nanoparticles supported on ceria and by Klyushin et al.[20] for the CO oxidation on Au supported catalyst. However, one must advert that carbides interact with metals much stronger than oxides with the direct formation of a strong bond between the Ni particle and the TiC support (see below) that produces a noticeable electronic perturbations on the supported particle. Precisely, the intricate interplay between the metal and the support has been recently shown through extensive kinetic Monte Carlo simulations on the water gas shift reaction on Au nanoparticles supported on MoC that highlighted the role played by every part of the catalyst.[21] The number of cases evidencing a possible active role of the support is increasingly growing and it is now clear that metal support interactions can be used to tune a specific activity and selectivity.[22] Clearly, this requires a detailed description of the mechanism of the catalytic reaction that includes both metal and support. In this sense, a complete understanding of the metal-

support interactions is necessary to fully exploit this phenomenon and many research articles focus precisely on the properties of nickel nanoparticles supported on metal oxides.[23-31]

In principle, when designing novel catalysts, metal-support interactions can be used to modify the chemical properties and the dispersion of a metal, but it is necessary the use of supports which are truly active in the binding of the metal. Among the possible materials that can be used as supports in catalysis, transition metal carbides (TMCs)[32] have emerged as a good alternative (vide infra) to oxide surfaces, which usually need defects or O vacancies to interact well with a dispersed metal. TMCs have long attracted the attention of the catalysis community since these materials combine physical properties of three different classes of materials. They present the extreme hardness peculiar of covalent solids, the excellent electric and thermal conductivity of a metal and the high melting points usual of ionic crystals.[32,33] TMCs have been proposed as alternative catalysts to noble metal because they display catalytic activities similar or even better than Pt-group metals.[34-37] These materials are also increasingly investigated in electrocatalysis, both in the hydrogen evolution[38-41] and oxygen reduction[42] reactions. As mentioned above, TMCs have been rather recently introduced as possible supports for metallic nanoparticles displaying good activity and selectivity. In particular, Au nanoparticles supported on TiC, but also Cu and Ni supported on TiC and on other TMCs such as MoC and Mo_2C, have been shown excellent activity in desulfurization processes,[43-47] O_2 dissociation,[48-50] H_2 dissociation,[51] CH_4 dissociation,[52] CO_2 hydrogenation[53,54] and WGSR.[21] It is worth emphasizing that Ni nanoparticles on TiC have shown good activity for CO_2 conversion,[55] although many details of the mechanism remain unknown, starting with the effect of the TiC support on the atomic and electronic properties of the Ni nanoparticles. This, at variance with other cases that have been previously studied,[56-58] introduce new aspects related to the magnetic properties arising from incomplete 3d shells. Ni nanoparticles are attracting a lot of attention for the hydrogenation of CO_2 because, in addition to being non-expensive, depending on their size and interaction with the support they can yield CO, CH_4, higher alkanes or methanol as the main reaction product. Thus, one has a system which can be catalytically tuned in terms of activity and selectivity.

In the present work, we investigate the interaction between nickel nanoparticles and a TiC support and compare to previous studies focusing on other metallic nanoparticles on the same TiC support. We also compare the present results with those reported previously for nickel nanoparticles supported on metal oxides. From this comparison, new features emerge that may help to develop new and more efficient catalysts for greenhouse gas conversion. In particular, the choice of magnetic nanoparticles turns out to be especially useful as it reveals that the metal atoms at the interface are likely to be responsible for the catalytic activity that has been reported for these systems.

Computational details and surface models

The interaction between different types of two-dimensional (2D) and three-dimensional (3D) Ni nanoparticles and the TiC(001) surface has been investigated by means of density functional theory (DFT) based calculations applied to suitable periodic models that are described in detail below.

All calculations have been performed using the Vienna Ab Initio Simulation Package (VASP) code [59-61] where the valence electron density is expanded in a plane wave basis set and the atomic cores are represented by projector augmented wave (PAW) method.[62] The BEEF-vDW exchange correlation functional,[63] that includes non-local correlation and dispersion effects, has been chosen since several benchmark studies [63-65] have shown that it provides a better agreement with the available experimental data than other typical functionals. Except for the bare TiC surface model, spin-polarization is always taken into account, a requirement due to the existence of magnetic moments in the nickel atoms arising from its incomplete occupation of the 3d shell.

The TiC(001) surface has been modelled by a slab supercell model including four atomic layers. In the past, a slab of this thickness has shown to be useful for studying of the interaction of metals and molecules with the TiC(001) substrate.[49,66] Depending on the size of the supported Ni nanoparticles, different supercell sizes have been used to avoid interactions between periodically repeated nickel nanoparticles. In a similar way, a vacuum width of at least a 12 Å has been used to minimize spurious interactions between periodically repeated slabs in the perpendicular direction to the surface. In all calculations, a cut-off energy of 415 eV has been used for the plane wave expansion, while the size of the Monkhorst-Pack[67] ***k***-points mesh used for sampling the first Brillouin zone has been varied adapted to the size of the slab supercell as explained below. The electronic energy convergence criterion has been selected to 10^{-5} eV while the geometry optimization (ionic relaxation) has been iterated until all forces acting on atoms were smaller than 0.01 eV $Å^{-1}$. For all the calculations nickel nanoparticles were allowed to fully relax in the geometry optimization calculations, while the number of titanium carbide layers able to relax varied depending on the surface size.

Five different slab models consisting of a titanium carbide surface with adsorbed nickel nanoparticles have been considered. These include three 2D nickel nanoparticles (Ni_4, Ni_9 and Ni_{16}) and two 3D (Ni_{13} and Ni_{29}) nickel nanoparticles. For the smallest (Ni_4), medium (Ni_9 and Ni_{13}) and largest (Ni_{16} and Ni_{29}) supported nickel nanoparticles considered in the present work. Several sites were explored for the supported particles with Ni atoms on top of Ti, on top of Ti-Ti bridge sites and on top of C, the latter being the most stable, as expected, with the final structures obtained being in

line with other theoretical and experimental observation for Au nanoparticles supported on TiC.[46,47] Note that the focus here is in the electronic properties of the supported clusters similar to those that are observed by STM, thus neglecting dynamic aspects that can lead to sintering. This is no doubt an important issue that is out of the scope of the present work.

The TiC(001) surface has been modelled with a 3×3, 4×4 and 5×5 TiC supercell, respectively. The Monkhorst-Pack[67] $\boldsymbol{k}$-point mesh used on the calculations was ($5 \times 5 \times 1$), ($3 \times 3 \times 1$) and ($1 \times 1 \times 1$) for the small, medium and large supercells, respectively. For the small and medium size models the two bottom layers have been kept fixed in their bulk positions, while for the larger slabs the three bottom layers have been kept fixed. This is justified as the calculations for the small and medium supercells do not show significant relaxation of the subsurface atomic layers. The remaining outermost layers and the nickel nanoparticles have been allowed to fully relax during the geometry optimization calculation. The calculations for the isolated Ni_n nanoparticles were carried out placing the nanoparticles in an asymmetric box at the **Γ**-point. The dimension of the box is ($11 \times 12 \times 13$) Å^3, ($13 \times 14 \times 15$) Å^3 and ($17 \times 18 \times 19$) Å^3 for the smallest, medium and largest nanoparticles, respectively. The choice of an asymmetric box is to ensure that the orbital filling does not involves dealing with near degeneracies. Yet, one must be aware that switching occupied and virtual orbital can lead to a nearly degenerate electronic state. The initial geometries used for the gas-phase nickel nanoparticles are those reported as the most stable in previous works.[68,69] Note that whenever two different geometries are reported for a given nanoparticle, two calculations have been carried out to obtain the most stable nanoparticle. For a better rationalization of the metal-support interactions, pertinent Density of States (DOS) calculations have been done using the smearing method proposed by Methfessel-Paxton[70] with a denser $\boldsymbol{k}$-point mesh. Finally, a charge density difference analysis has been carried out by means of the VESTA software;[71] this turns out to be an excellent way to quantify charge transfer between the metal and the support.

Several different properties related to the gas-phase and adsorbed nanoparticles have been investigated. First, we consider the cohesive energy (E_{coh}) of the gas-phase Ni_n nanoparticles defined as in Eq. (1),

$$E_{coh} = \frac{E_{Ni_n}}{n} - E_{Ni} \qquad (1)$$

where E_{Ni_n} is the energy of the gas-phase Ni_n nanoparticle and E_{Ni} is the energy of the isolated nickel atom in gas-phase. The adsorption energy (E_{ads}) of the Ni_n nanoparticles has been calculated as in Eq. (2),

$$E_{ads} = E_{Ni_n - TiC} - E_{Ni_n} - E_{TiC} \quad (2)$$

where $E_{Ni_n - TiC}$ is the energy of the supercell containing the nickel nanoparticle adsorbed on the TiC surface and E_{TiC} is the energy of the relaxed pristine TiC(001) surface. Note that with this definition, the more negative E_{ads}, the stronger the interaction. Finally, the adhesion energy (E_{adh}) is calculated as follows:

$$E_{adh} = E_{Ni_n - TiC} - E_{Ni_n, opt\ geom} - E_{TiC, opt\ geom} \quad (3)$$

where $E_{Ni_n, opt\ geom}$ and $E_{TiC, opt\ geom}$ are the energies of the isolated nickel nanoparticle and of the isolated surface both at the optimized geometry upon adsorption, respectively. Here, as for E_{ads}, the more negative E_{adh}, the stronger the interaction. It is work pointing out that the adhesion energy is normally reported per unit area assuming that the interaction is merely due to the atoms in direct contact with the surface. Here, we report the adhesion energy per number of nickel atoms in direct contact; thus, representing the same magnitude. Note that the adhesion energy could be described also as

$$E_{adh} = E_{ads} - E_{Ni_n}^{def} - E_{TiC}^{def} = E_{ads} - E^{def} \quad (4)$$

where $E_{Ni_n}^{def}$ and E_{TiC}^{def} are the deformation energy of the Ni_n nanoparticle and the deformation energy of the TiC carbide surface upon adsorption; the sum of the two contributions is denoted as E^{def}. For comparison, the adsorption, adhesion and deformation energies will be reported normalized per atom in contact with the surface.

Results and discussions

Gas-phase Ni_n nanoparticles were optimized using as initial guesses previously available data[68,69] and whenever two different structures were reported, optimization of both structures was done to obtain the optimum structure. The most stable gas-phase nanoparticles are presented in Figure 1 and structural details are given in Electronic Supplementary Information (ESI). The results show that even the smallest gas-phase nickel nanoparticles adopt a 3D conformation. This is not always observed for all the transition metals as it is known that small Cu and Au clusters exhibit a planar conformation.[56,68] The cohesive energy of all gas-phase nickel nanoparticles are summarized on Table 1, where values for fcc bulk Ni are included for comparison. In fact, the calculated bulk cohesive energy agrees with the experimental value,[72] which is in line with previous results obtained using GGA, meta-GGA and hybrid density functionals.[73,74] Moreover, as expected, the cohesive energy nicely converges to the bulk value with the nanoparticles increasing size. Another important property of the Ni nanoparticles

is their magnetic moment, which is reported in the leftmost column of Table 2. The total magnetic moment increases with the number of Ni atoms, as expected. A more interesting magnitude is the magnetic moment per Ni atoms; this is largest for the smallest Ni_4 cluster but converges quite fast towards the bulk values. The convergence to the bulk value is because the largest the average coordination number the lowest the average magnetic moment, and as the gas-phase nanoparticle grows, the average coordination number increases. As expected, the calculated magnetic moments are in good agreement with previous studies[68,69] since the gas-phase geometries were already very similar.

In general, the deposition of a metal particle on a support could induce modifications in its structure as a consequence of strong metal-support interactions, which might overcome the effects of metal-metal bonding. In our study, the metal-support interaction has been studied for the five different nickel nanoparticles already described, which ranges from small to medium experimental sizes, adopting 2D and 3D morphologies. The reason for this particular choice is that experimental evidence shows that at low coverage, transition metal nanoparticles adsorbed over TMCs tend to acquire planar structures, while for larger coverages they become 3D.[47,50] The structure of the adsorbed nanoparticles is displayed in Figure 2 and reported in the ESI. In all cases the Ni nanoparticles adsorb with the metal atoms above the C atoms of the TiC support, acquiring a distorted morphology but exhibiting clearly (001) facets. The smallest nanoparticles are flat, in line with the shape observed for small Au-TiC and Cu-TiC,[45,47,48,56,57] and as the size increases they become 3D as observed for the Au-TiC system.[47,50] Particularly, the Ni_{16} nanoparticle has two metastable atomic configurations with a difference of 0.05 eV in the total energy difference only. One of the isomers exhibits a square shape and (001) facets and the structure of the second one can be understood as the aggregation of four Ni_4 nanoparticles; hereafter this second structure will be denoted as $Ni_{16,rec}$. Therefore, the structures of Ni nanoparticles supported on TiC do not follow the trend observed for metal oxide supports such as ZrO_2, TiO_2, CeO_2 and MgO, where 3D structures have been reported even for small nanoparticles,[23-25,28-31] with the bottom nickel atoms interacting mostly with the oxygen atoms of the surface. Nevertheless, Mao et al.[31] did not find remarkable stability differences for the Ni_4 flat and Ni_4 3D nanoparticles adsorbed over CeO_2 though the 3D nanoparticle was found to be the most stable.

Next, we discuss the adsorption, adhesion and deformation energy per atom in contact with the surface as defined in the previous section and summarized in Table 3. Note that with this definition we consider that the Ni atoms in direct contact with the TiC surface are those contributing mainly to the adsorption and adhesion of the overall nanoparticle. From Table 3 it can be seen that the larger the number of Ni atoms in similar structures (2D or 3D) the lower the adsorption energy. Besides, a more pronounced change on the adsorption energy when increasing the size of the nanoparticles is found for

the 2D structures than for the 3D structures. The first observation could be rationalized because the larger the gas-phase nanoparticle the more stable it is with a concomitant decrease on the bonding capability. On the contrary, the smaller the nanoparticle the larger its bonding capability. The second observation could be understood as the energy required to reorganize the nanoparticle structures being larger for the 2D nanoparticles than for the 3D. Compared to other metals on TiC, the calculated adsorption energy per atom for the Ni_4 nanoparticle is lower than that of Pd_4 and Pt_4 on TiC but higher than that of Cu_4, Ag_4 and Au_4 on TiC reported by Gomez et al.[75], which nicely follow the trend that Pt-group metals adsorb stronger on TiC than Au-group elements. Note that the adsorption energies calculated by Gomez et al.[75] using a GGA (PW91) functional are relative to the gas-phase rhombus structure, while our calculations are with respect to the tetrahedral structure. This could lead to a slightly lower Pd_4-TiC adsorption energy since the most stable structure on gas-phase is also tetrahedral.[68] It is also interesting to compare the effect of the substrate. To this end, we compare our calculated adsorption energies for nickel nanoparticles on TiC with those reported for similar Ni nanoparticles supported on metal oxides. A first noticeable difference is that the interaction of Ni nanoparticles with the TiC support is stronger than those reported for non-reducible oxides such as MgO. Giordano et al.[28] reported an adsorption energy of the tetrahedral Ni_4 nanoparticle on MgO(001) of -1.17 eV $atom^{-1}$, somehow smaller values were reported by Di Valentin et al.[29] for the square planar Ni_4 and the 3D Ni_9 nanoparticles adsorbed over MgO(001); -0.28 and -0.48 eV $\cdot atom^{-1}$, respectively. The same trend is found for the tetrahedral Ni_4 nanoparticle adsorbed over ZrO_2 which is also a non-reducible oxide; the reported adsorption energy was of -0.47 eV $atom^{-1}$.[25] Not surprisingly, the adsorption energy becomes larger for a reducible oxide since charge-transfer between the particle and the adsorbate becomes chemically favoured. Thus, Mao et al.[31] and Wang et al.[26] found that the adsorption energy of the flat and tetrahedral Ni_4 nanoparticle adsorbed over CeO_2 and TiO_2 were of -1.34 and -1.00 eV $atom^{-1}$ and -1.43 and -1.02 eV $atom^{-1}$, respectively. Note that, for a better comparison, all literature values discussed above have been normalized with respect to the number of Ni atoms that are in contact with the oxide surface. As can be seen from Table 3, the interaction between Ni nanoparticles and TiC per Ni atom in contact with the surface is even larger than for reducible oxides.

Regarding the adhesion energy values presented in Table 3, not marked differences are observed for the different nanoparticle sizes, meaning that the different nanoparticles interact similarly with the surface, although Ni_4 is the one that has a strongest interaction, hence the highest adhesion energy. Interestingly, for the cases where the Ni nanoparticle has the same number of contact atoms with the surface, namely Ni_9 and Ni_{13} or Ni_{16} and Ni_{29}, the larger nanoparticle has a slightly higher

adhesion energy that could be explained because the uppermost atoms add a small contribution to the interaction with the surface. Concerning the deformation energies, note also that, according to Eq. (4), it contains two contributions. The major contribution to the deformation energy is mostly related to the gas-phase nickel nanoparticle while the TiC surface it is almost not deformed. The differences in the deformation energy contribution of the Ni nanoparticles with respect to the nanoparticle size are larger than for the adhesion energies. From Table 3 it appears that the Ni_4 nanoparticle is the one with the smallest deformation energy. This is because, when going from the gas-phase tetrahedral conformation to the adsorbed rhombohedral conformation, the structural change implies one atom only. For the larger nanoparticles the number of atoms that have to be reorganized is also larger, hence the deformation energy increases. Comparing the nanoparticles with the same number of contact atoms, the 3D nanoparticles have lower deformation energies. Again, this is because the number of atoms that have to be reorganized is smaller than in the 2D nanoparticles. Compiling all the information from Table 3 it is concluded that the Ni_4 nanoparticles should be the most stable and easiest to form nanoparticles on top of the TiC surface because they exhibit the largest adhesion and adsorption energies. Similarly, for those nanoparticles which are different in size but contain the same number of atoms in contact with the surface, the 3D ones are more stable and easier to form because of the highest adhesion and adsorption energies. This has implications for the modelling and also to understand the results of the experiments for CO_2 hydrogenation on Ni nanoparticles supported on TiC[55]. The variations in the structural properties of the Ni particles open the possibility to different ways to bind and activate CO_2, which could lead to different reaction products in the hydrogenation process (e.g., CO, CH_4, higher alkanes or methanol).

To complete the study, we focus now on the effect that the support has on the magnetic properties of the Ni nanoparticles. The interest here is because, in principle, any catalytic reaction involving radical species can be affected by a change in the spin alignment and magnetic properties of a metal centre. To disentangle support and structural effects we consider the magnetic moment of three different structures; the gas-phase Ni nanoparticle ($\mu_{Ni,g}$), the Ni nanoparticle in the gas-phase but at the adsorbed geometry ($\mu_{Ni,eq}$), and the Ni nanoparticle adsorbed over the surface ($\mu_{Ni,ads}$). The trend for the gas-phase nanoparticles has already been discussed and we just recall that the magnetic moment per atom converges quite rapidly to the calculated bulk value, which is also close to experimental value of 0.6 μ_B.[72] Table 2 shows that, in general, the magnetic moments of the Ni nanoparticles at the equilibrium adsorption structures ($\mu_{Ni,eq}$) are quite higher than the corresponding values in the gas-phase equilibrium geometry ($\mu_{Ni,g}$). This support effect can be easily rationalized because the coordination number of the Ni nanoparticles at the supported geometry is smaller than for the gas-

phase structure. Remarkably, the supported Ni nanoparticles exhibit the lowest magnetic moments ($\mu_{Ni,ads}$). This is a clear indication of a chemical interaction between the Ni nanoparticle and the support. This interaction, involving a covalent bonding through Ni(3d) and C(2p) orbitals mixing, is strong enough to quench the increase of magnetic moment induced by the structural change upon adsorption. As seen for the other cases, the largest the adsorbed nanoparticle, the lowest the magnetic moment per atom as the average coordination number of the nickel atoms increases. Note also that the Ti and C surface atoms of the TiC substrate do not exhibit any magnetic moment, and this does not change upon adsorption of the nickel nanoparticles. Interestingly, the coordination number effect is also observed when comparing the Ni_{16} and $Ni_{16,rec}$ nanoparticles, the former exhibiting a higher average coordination number and also a lower magnetic moment. Finally, it is also interesting to point out that for the 3D nanoparticles, the uppermost atoms have a larger magnetic moment while for the atoms in direct contact this is lower. This is in agreement with the conclusion above mentioned that the metal-support interaction induces a quenching of the magnetization of the supported nanoparticle. This conclusion contrasts with the findings of previous studies for Ni nanoparticles supported on MgO(001). Giordano et al.[28] found that the magnetic moment per atom of the tetrahedral Ni_4 nanoparticle supported over MgO was 1.0 μ_B, the same observed for the gas-phase species. Later on, Di Valentin et al.[29] reported a magnetic moment for the flat Ni_4 and 3D Ni_9 nanoparticles adsorbed over MgO to be 1.40 and 0.89 μ_B , again the same as in the gas-phase nanoparticles. The fact that the values reported for Ni nanoparticles supported on MgO are higher than the present ones for similar nanoparticles supported on TiC, is a clear indication of the existence of a chemical interaction between the Ni nanoparticles and the TiC surface, which is not present when the support is MgO, where the leading interactions are electrostatic with an expected contribution of dispersion.

To further understand the metal-support interaction we have carried out a Bader analysis[76] and computed the net charge for the Ni atoms in the nanoparticle as well as for the atoms in the support. Interestingly, there are no relevant changes in the net charges indicating that there is no noticeable charge transfer between the Ni nanoparticles and the TiC. A similar result was encountered long ago for the interaction of Au nanoparticles with the TiC surface; no clear sign of charge transfer but a clear polarization of the Au nanoparticle electron density produced by the support that has a clear fingerprint in the C(1s) X-ray Photoemission Spectra.[56] To further analyse the nature of the interaction between the Ni nanoparticles and the TiC support we have also obtained the density of states (DOS) and charge density difference plots. In particular, a local density of states (LDOS) and partial density of states (PDOS) have been carried out for the clean TiC surface and the Ni_n-TiC systems. On the calculations we have considered the upper layer of the titanium carbide surface and the overall nickel nanoparticles

focussing on the Ti_{3d}, C_{2p} and Ni_{3d} states, as summarized in Figure 3. From Figure 3 the region near the Fermi level for the clean TiC is flatter than when the nanoparticle is adsorbed because there are some Ni_{3d} populated states around this region. Moreover, for the Ni_n-TiC systems there are some pronounced peaks near the Fermi level that are related to a mixing of the C_{2p}, Ti_{3d} and Ni_{3d} states; thus, showing a chemical interaction between the nanoparticles and the surface. Furthermore, for the 3D nanoparticles it could be seen that the uppermost nickel atoms also mix with the C_{2p} and Ti_{3d} states, although in a lesser extent than the interfacial atoms. This confirm that the higher interaction in the 3D nanoparticles is due to the additional contribution of Ni atoms in the uppermost atomic layers.

Finally, we have performed a charge density difference analysis to evaluate the metal-support interaction, which is reported in Figure 4. The charge difference is defined as

$$\rho = \rho_{Ni_n - TiC} - \rho_{Ni_n,\, opt\ geom} - \rho_{TiC,\, opt\ geom} \quad (5)$$

where $\rho_{Ni_n - TiC}$, $\rho_{Ni_n,\, opt\ geom}$ and $\rho_{TiC,\, opt\ geom}$ are the electron density of the adsorbed nanoparticle over the surface, the isolated nanoparticle at the optimum adsorption geometry and the titanium carbide surface at the optimum adsorption geometry, respectively. From Figure 4 it could be seen that for all the nanoparticles there is an accumulation of charge density on top of the nickel atoms while there is a charge depletion on the hollow sites. There is clear chemical interaction even if the net charge transfer is negligible. Moreover, for the 3D structures the uppermost layers have lower charge density accumulation since they interact less with the surface as shown in the DOS diagrams. As a matter of fact, it could be seen that the third layer of the Ni_{29} structure is almost non-perturbed by the titanium carbide surface. This is in agreement with previous works indicating that the catalytic activity of metals on TiC is due to the presence of flat and small supported nanoparticles.[44-52]

Conclusions

Metals supported on transition metal carbides are known to exhibit good catalytic activity and selectivity in a rather large list of reactions. For metals such as Cu and Au, the increased catalytic activity has been attributed to the polarization of their electron density in response to the presence of the underlying carbide.[47,51,77] However, in the case of magnetic nanoparticles the available information is almost inexistent. To fill this gap in our understanding of catalysts based on metals supported on transition metal carbides we investigated in detail the effect that a TiC support has in the structural, electronic, and magnetic properties of Ni nanoparticles. By means of periodic DFT calculations using suitable supercells three two-dimensional (Ni_4, Ni_9 and Ni_{16}) and two three-dimensional (Ni_{13} and Ni_{29}) nanoparticles of increasing size have been selected as representative examples.

The obtained results plus a detailed comparison to earlier studies involving other metals on the TiC support or Ni nanoparticles on other supports allowed us to reach a series of firm conclusions. First, the smallest Ni_4 nanoparticles exhibit the largest adsorption and adhesion energies. The large stability of these supported nanoparticles together to the large adsorption energies indicates that these are likely to be abundant in Ni/TiC systems prepared by vapor deposition;[55] a conclusion which is in agreement with the prediction that such a small Ni nanoparticles supported on TiC are active for methane dissociation even at room temperature.[52] Second, the three-dimensional nanoparticles are more stable and easier to form than their homologous two-dimensional counterparts. Third, Ni_4 and Ni_9 appear to interact with the TiC substrate stronger than as reported for non-reducible and reducible oxides such as MgO and CeO_2, respectively. Additionally, for the Ni_4-TiC nanoparticle we have confirmed the trend that Pt-group nanoparticles adsorb stronger than Au-group nanoparticles over TiC surfaces. Finally, we presented evidence that, while the distortion of the structure of the supported nanoparticles induced by the support increases the average magnetic moment per Ni atom, the overall result is a considerable quenching of the magnetic moment. This is a feature not observed in nickel nanoparticles supported on MgO and a clear indication of the presence of chemical interaction between the Ni nanoparticles and the TiC support. This is confirmed by the analysis of the three-dimensional nanoparticles, where the largest magnetic moment corresponds to atoms in the uppermost layers. The fact that the magnetic moment in the uppermost layers remains as in the isolated nanoparticle indicates that the chemical activity of these atoms is almost not affected by the presence of the TiC support and that the active sites will be those at the interface, thus giving support to previous studies focusing on this type of models. The DOS and the charge density difference analysis also reveal the existence of chemical interactions between the Ni nanoparticle and the TiC support, even if the net charge transfer between the two systems is negligible.

The reported results have been obtained for a TiC support but, in the view of the similarity in the electronic structure of other transition metal carbides with 1:1 stoichiometry and rock-salt crystal structure, it is likely that the present findings will apply to systems composed of other magnetic nanoparticles and different transition metal carbides, which also have implications in the catalytic properties of the resulting systems. Furthermore, from these results, it is clear that a carbide support can be quite useful to modify the chemical properties and the dispersion of a metal while designing novel catalysts.

.

Table 1. Calculated cohesive energy (E_{coh}) of gas-phase Ni_n nanoparticles, Ni bulk and experimental Ni bulk value.

Structure	E_{coh} / eV atom^{-1}
Ni_4	-1.88
Ni_9	-2.56
Ni_{13}	-2.75
Ni_{16}	-2.85
Ni_{29}	-3.13
Ni bulk	-4.28
Ni bulk Experimental [72]	-4.44

Table 2. Total magnetic moment of Ni_n nanoparticles at the gas-phase nickel ($\mu_{Ni,g}$), at the adsorbed geometry but without being adsorbed ($\mu_{Ni,eq}$) and when adsorbed ($\mu_{Ni,ads}$). Results in parentheses correspond to the average magnetic moment per Ni atom. All results are in Bohr magneton units (μ_B). The calculated value for bulk Ni is 0.65 $\mu_B$which is close to the experiment figure of 0.6 μ_B.[72]

	$\mu_{Ni,g}$	$\mu_{Ni,eq}$	$\mu_{Ni,ads}$
Ni_4	4.00 (1.00)	5.14 (1.29)	1.85 (0.46)
Ni_9	8.00 (0.89)	8.00 (0.89)	3.52 (0.39)
Ni_{13}	10.00 (0.77)	11.43 (0.88)	4.58 (0.35)
Ni_{16}	12.00 (0.75)	16.06 (1.00)	2.29 (0.14)
$Ni_{16\ reconstructed}$	12.00 (0.75)	16.03 (1.00)	5.50 (0.34)
Ni_{29}	20.00 (0.69)	22.22 (0.77)	10.38 (0.36)

Table 3. Adsorption (E_{ads}), adhesion (E_{adh}) and deformation (E_{def}) energies per atom of nickel in direct contact for the different Ni_n nanoparticles. The total number of nickel atoms in direct contact with the surface is given in parenthesis. For sake of simplicity, $Ni_{16,rec}$ values have not been included.

	E_{ads} / eV atom^{-1}	E_{adh} / eV atom^{-1}	E_{def} / eV atom^{-1}
Ni_4 (4)	-1.76	-2.07	0.31
Ni_9 (9)	-1.16	-1.85	0.69
Ni_{13} (9)	-1.58	-1.99	0.41
Ni_{16} (16)	-0.88	-1.92	1.04
Ni_{29} (16)	-1.41	-2.00	0.59

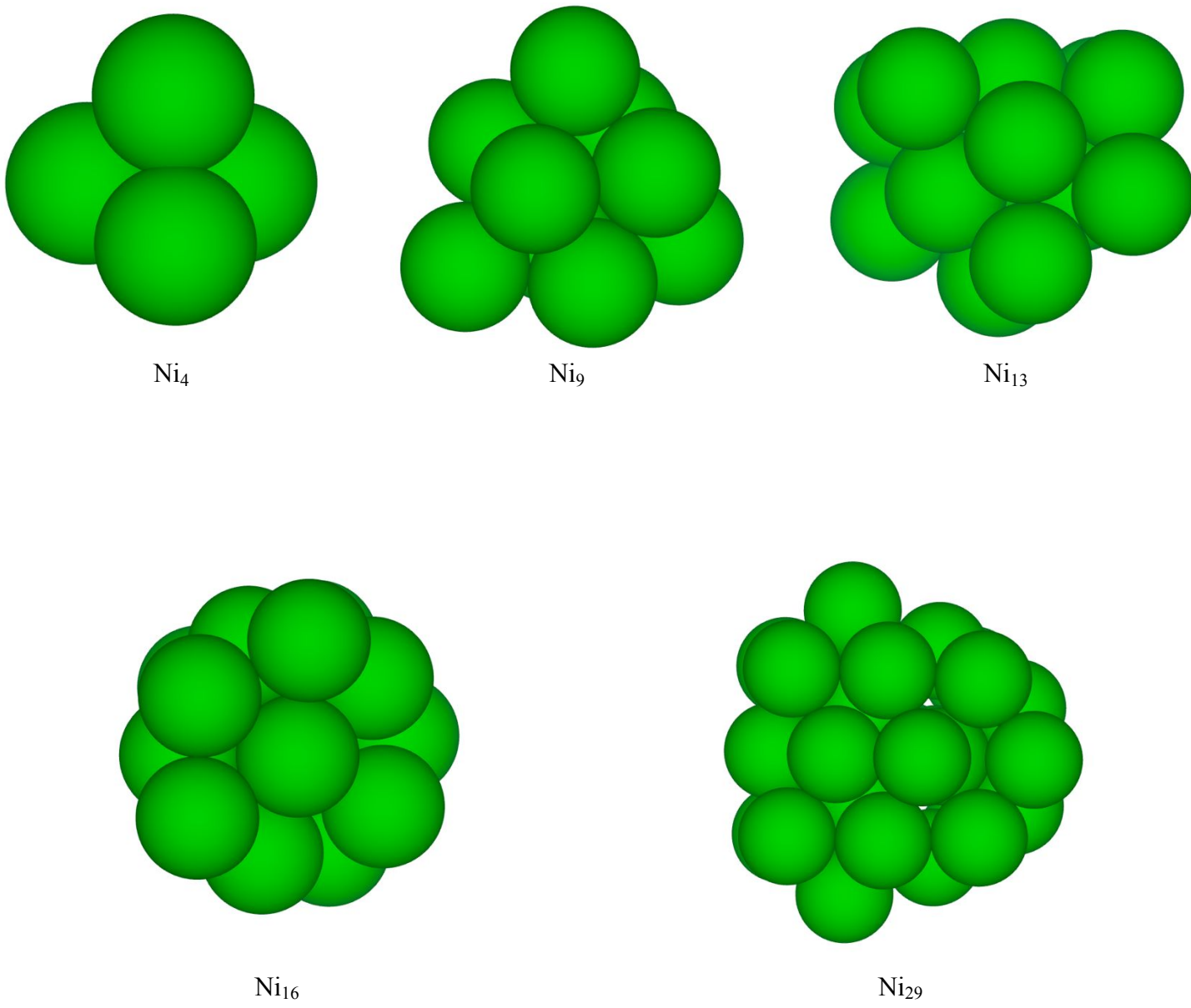

Figure 1. Atomic structure of the most stable gas-phase Ni_n nanoparticles.

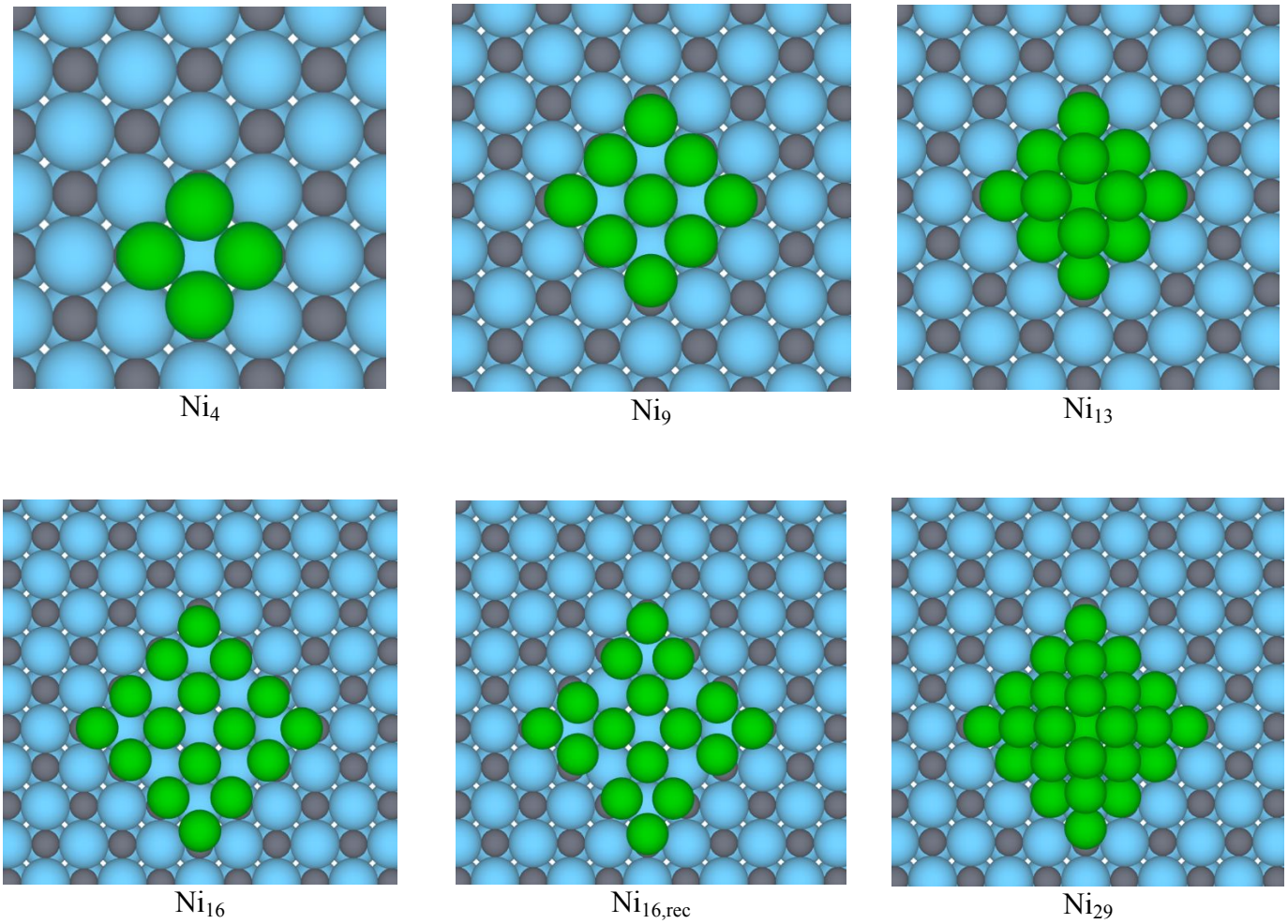

Figure 2. Ni_n nanoparticles adsorbed over the (001) titanium carbide surface. Light blue, grey and green colours are used for titanium, carbon and nickel, respectively. Note that Ni_{13} and Ni_{29} are 3D nanoparticles.

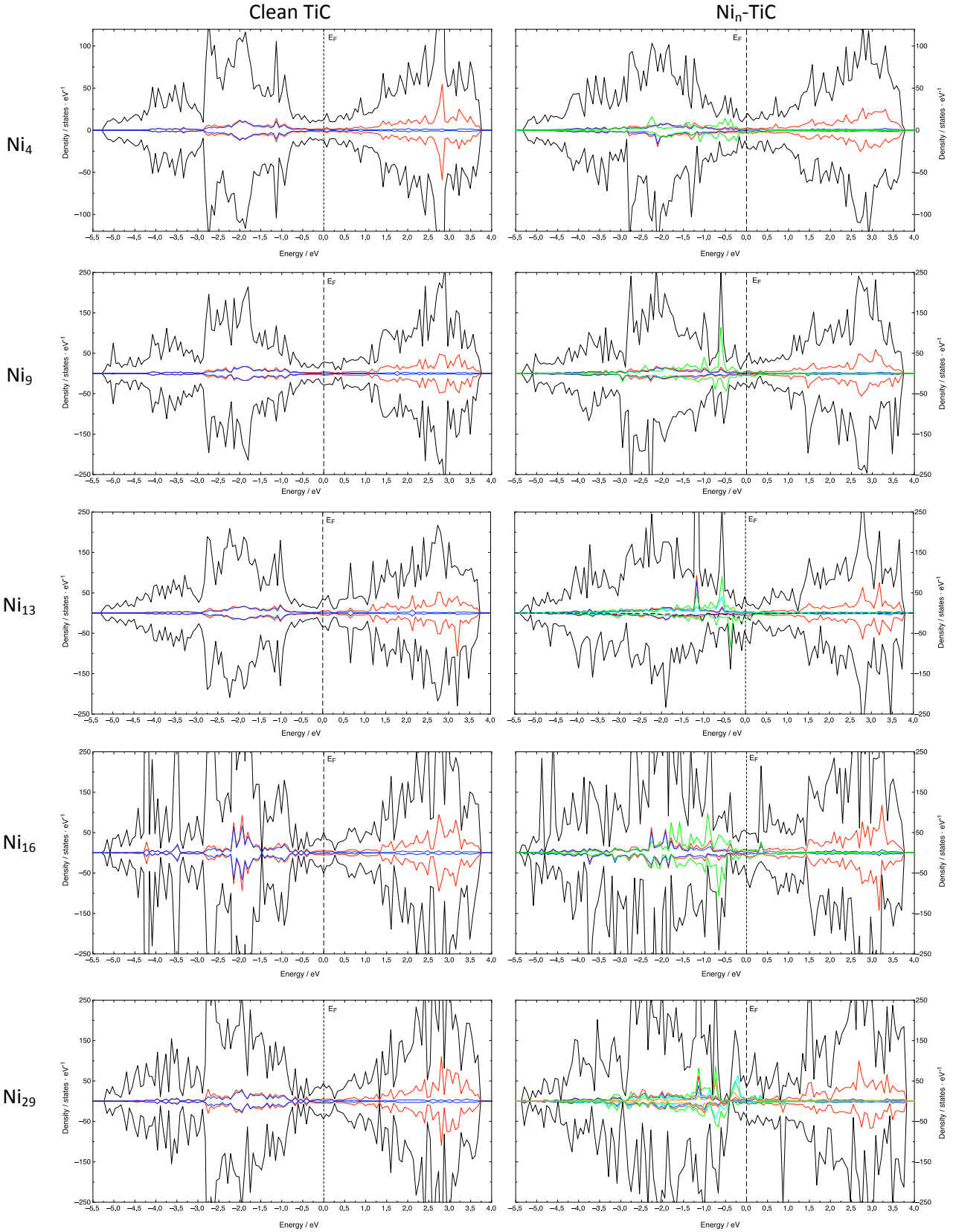

Figure 3. Density of states diagram for the clean TiC surface and the Ni_n-TiC nanoparticles. Black colour represents the total DOS contribution and red, blue and green colours represent the contribution

of the Ti_{3d}, C_{2p} and Ni_{3d} states, respectively. For the 3D nanoparticles light blue and orange colours represent Ni_{3d} states of the second and third layer, respectively. Dash line represent the Fermi level. Note that we have only considered the contribution of the outermost TiC layer and all the nickel atoms contribution.

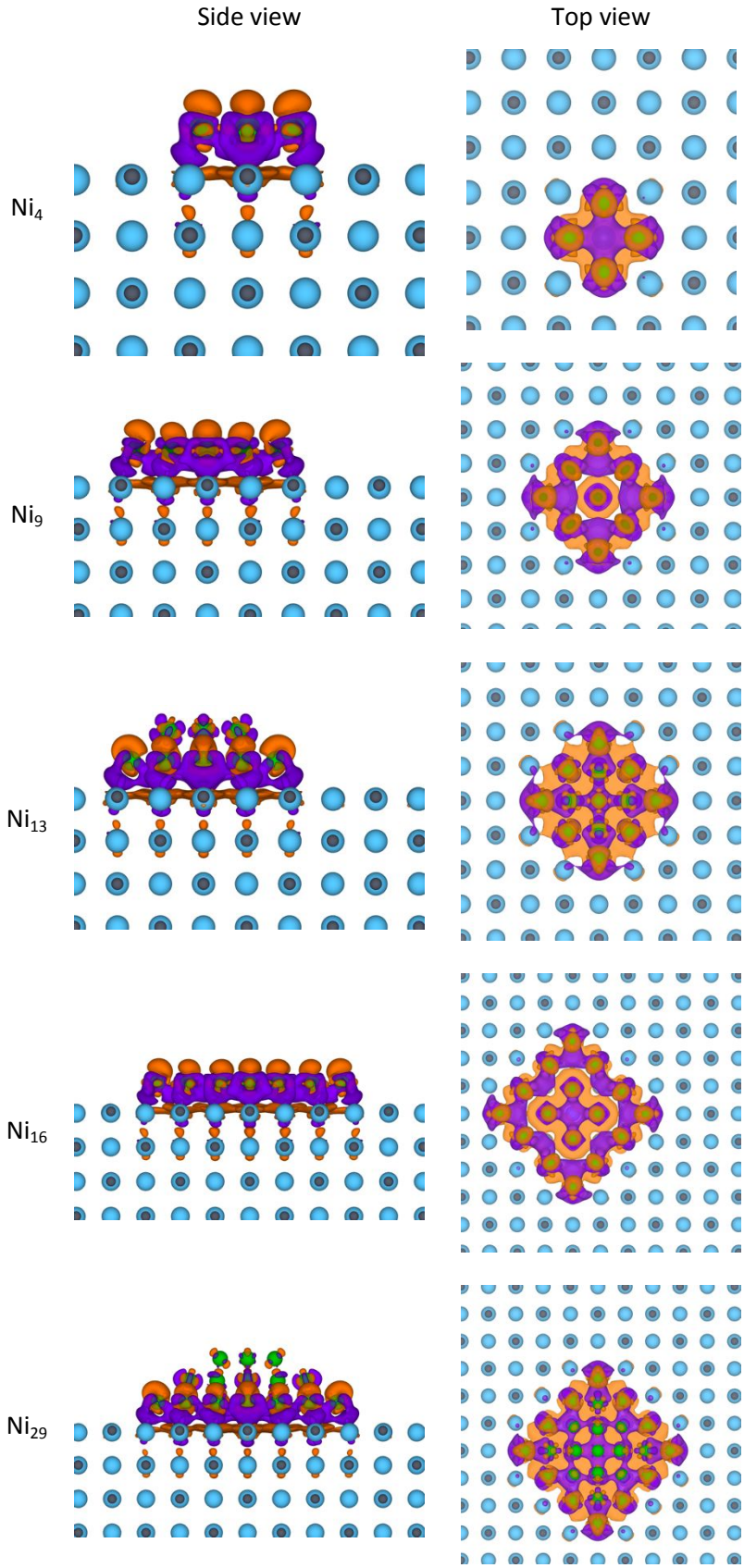

Figure 4. Charge density difference maps for Ni_n-TiC. Light blue, grey and green colours are used for titanium, carbon and nickel, respectively. The isosurface is taken as 0.0033 e^-/bohr^3. Orange regions denote accumulation of charge density, while purple regions denote charge density depletion.

Conflicts of interest

There are no conflicts of interest to declare.

Acknowledgments

The research at the *Universitat de Barcelona* has been supported by the Spanish Ministry of Science, Innovation and Universities (MICIUN) through grants RTI2018-094757-B-I00, RTI2018-095460-B-I00, MCIU/AEI/FEDER, UE and MDM-2017-0767, and in part, by the *Generalitat de Catalunya* (grant 2017SGR13). The work carried out at the Brookhaven National Laboratory (BNL) was supported by the U.S. Department of Energy, Office of Science and Office of Basic Energy Sciences under contract No. DE-SC0012704. P. L-R. acknowledges MICIUN for a predoctoral FPU18/02313 grant. F. I. acknowledges additional support from the 2015 ICREA Academia Award for Excellence in University Research. Computational resources provided by *Consorci de Serveis Universitaris de Catalunya* (CSUC, former CESCA) and *Red Española de Supercomputación* at the Barcelona Supercomputing Center (grants QS-2020-1-0003 and QS-2020-2-0009 are gratefully acknowledged

References

[1] J. M. Thomas and W. J. Thomas, *Principles and Practice of Heterogeneous Catalysis*, VCH, Weinheim, 1997.

[2] F. Barbir, *Energy*., 2009, **34**, 308–312.

[3] I. Dincer, *Renew. Sust. Energ. Rev*., 2000, **4** 157–175.

[4] M.A.A. Aziz, A.A. Jalil, S. Triwahyono, R.R. Mukti, Y.H. Taufiq-Yap and M.R. Sazegar, *Appl. Catal. B. Environ.*, 2014, **147** 359–368.

[5] F. Ocampo, B. Louis, L. Kiwi-Minsker and A.-C. Roger, *Appl. Catal. A. Gen*., 2011, **392**, 36–44.

[6] G. Zhou, H. Liu, K. Cui, H. Xie, Z. Jiao, G. Zhang, K. Xiong and X. Zheng, *Int. J. Hydrogen Ener*., 2017, **42**, 16108–16117.

[7] S. Hwang, U.G. Hong, J. Lee, J.H. Baik, D.J. Koh, H. Lim and I.K. Song, *Catal Lett*., 2012, **142**, 860–868.

[8] L. Yang, L. Pastor-Pérez, S. Gu, A. Sepúlveda-Escribano and T.R. Reina, *Appl. Catal. B. Environ.*, 2018, **232**, 464–471.

[9] F. Sun, C. Yan, Z. Wang, C. Guo and S. Huang, *Int. J. Hydrogen Ener*., 2015, **40**, 15985–15993.

[10] Y. Wang, L. Yao, Y. Wang, S. Wang, Q. Zhao, D. Mao and C. Hu, *ACS Catal*., 2018, **8**, 6495–6506.

[11] S. Ali, M.M. Khader, M.J. Almarri and A.G. Abdelmoneim, *Catal. Today*., 2020, **343**, 26–37.

[12] K. Delgado, L. Maier, S. Tischer, A. Zellner, H. Stotz and O. Deutschmann, *Catalysts.*, 2015, **5**,

871–904.

[13] M.M. Barroso-Quiroga, A.E. Castro-Luna, *International Journal of Hydrogen Energy*., 2010, **35**, 6052–6056.

[14] K. Lertwittayanon, W. Youravong and W.J. Lau, *Int. J. Hydrogen Ener*., 2017, **42**, 28254–28265.

[15] M. García-Diéguez, I.S. Pieta, M.C. Herrera, M.A. Larrubia and L.J. Alemany, *J. Catal*., 2010, **270**, 136–145.

[16] S. J. Tauster, S. C. Fung and R. L. Garten, *J. Am. Chem. Soc*., 1978, **100**, 170-175.

[17] S. J. Tauster, S. C. Fung, R. T. K. Baker and J. A. Horsley, *Science*, 1981, **211**, 1121-1125.

[18] S. J. Tauster, *J. Acc. Chem. Res*., 1987, **20**, 389–394.

[19] A. Bruix, J. A. Rodriguez, P. J. Ramírez, S. D. Senanayake, J. Evans, J. B. Park, D. Stacchiola, P. Liu, J. Hrbek and F. Illas, *J. Am. Chem. Soc*., 2012, **134**, 8968-8974.

[20] A. Y. Klyushin, T. E. Jones, T. Lunkenbein, P. Kube, X. Li, M. Hävecker, A. Knop-Gericke and R. Schlögl, *ChemCatChem*., 2018, **10**, 3985-3989.

[21] H. Prats, S. Posada-Pérez, J. A. Rodriguez, R. Sayós and F. Illas, *ACS Catal*., 2019, **9**, 9117-9126.

[22] T.W. van Deelen, C. Hernández Mejía and K.P. de Jong, *Nat Catal*., 2019, **2**, 955–970.

[23] A. Cadi-Essadek, A. Roldan and N.H. de Leeuw, *Faraday Discuss*., 2018, **208**, 87–104.

[24] A. Cadi-Essadek, A. Roldan and N.H. de Leeuw, *Fuel Cells*, 2017, **17**, 125–131.

[25] J. Yang, J. Ren, H. Guo, X. Qin, B. Han, J. Lin and Z. Li, *RSC Adv*., 2015, **5**, 59935–59945.

[26] Y. Wang, Y. Su, M. Zhu and L. Kang, *RSC Adv*., 2015, **5**, 16582–16591.

[27] A. Markovits, M.K. Skalli, C. Minot, G. Pacchioni, N. López and F. Illas, *J. Chem. Phys.*, 2001, **115**, 8172–8177.

[28] L. Giordano, G. Pacchioni, A.M. Ferrari, F. Illas and N. Rösch, *Surf. Sci.*, 2001, **473**, 213–226.

[29] C. Di Valentin, L. Giordano, G. Pacchioni and N. Rösch*, Surf. Sci.*, 2003, **522**, 175–184.

[30] J. Carrasco, L. Barrio, P. Liu, J.A. Rodriguez and M.V. Ganduglia-Pirovano, *J. Phys. Chem. C*., 2013, **117**, 8241–8250.

[31] Z. Mao, P.G. Lustemberg, J.R. Rumptz, M.V. Ganduglia-Pirovano and C.T. Campbell, *ACS Catal*., 2020, **10**, 5101–5114.

[32] H.H. Hwu and J.G. Chen, *Chem. Rev*., 2005, **105**, 185–212.

[33] L. E. Toth, *Transition Metal Carbides and Nitrides,* Academic, New York, 1971

[34] R.B. Levy and M. Boudart, *Science*, 1973, **181**, 547–549.

[35] I. Kojima, E. Miyazaki, Y. Inoue and I. Yasumori, *J. Catal*., 1979, **59**, 472–474.

[36] C. Jimenez-Orozco, E. Flórez, F. Viñes, J.A. Rodriguez and F. Illas, *ACS Catal*., 2020, **10**, 6213–6222.

[37] J.A. Rodriguez, P.J. Ramírez and R.A. Gutierrez, *Catal. Today*, 2017, **289**, 47–52.

[38] W.-F. Chen, J.T. Muckerman and E. Fujita, *Chem. Commun*., 2013, 49, 8896.

[39] F. Harnisch, G. Sievers and U. Schröder, *Appl. Catal. B. Environ*., 2009, **89**, 455–458.

[40] D. Ham, R. Ganesan and J. Lee, *Int. J. Hydrogen Ener.*, 2008, **33**, 6865–6872.

[41] S. Wirth, F. Harnisch, M. Weinmann and U. Schröder, *Appl. Catal. B. Environ*., 2012, **126**, 225–230.

[42] A. Ignaszak, C. Song, W. Zhu, J. Zhang, A. Bauer, R. Baker, V. Neburchilov, S. Ye and S. Campbell, *Electrochim. Acta*, 2012, **69**, 397–405.

[43] P. Liu and J.A. Rodriguez, *J. Chem. Phys.*, 2003, **119**, 10895–10903.

[44] J.A. Rodriguez, P. Liu, Y. Takahashi, F. Viñes, L. Feria, E. Florez, K. Nakamura and F. Illas, *Catal. Today*, 2011, **166**, 2–9.

[45] L. Feria, J.A. Rodriguez, T. Jirsak and F. Illas, *J. Catal*., 2011, **279**, 352–360.

[46] J.A. Rodriguez, P. Liu, Y. Takahashi, K. Nakamura, F. Viñes and F. Illas*, J. Am. Chem. Soc*., 2009, **131**, 8595–8602.

[47] J.A. Rodriguez, P. Liu, F. Viñes, F. Illas, Y. Takahashi and K. Nakamura, *Angew. Chem*., 2008, **120**, 6787–6791.

[48] J.A. Rodriguez, P. Liu, J. Dvorak, T. Jirsak, J. Gomes, Y. Takahashi and K. Nakamura, *J. Chem. Phys*., 2004, **121**, 465-474.

[49] F. Viñes, C. Sousa, F. Illas, P. Liu and J.A. Rodriguez, *J. Phys. Chem. C*., 2007, **111**, 16982–16989.

[50] J.A. Rodríguez, L. Feria, T. Jirsak, Y. Takahashi, K. Nakamura and F. Illas, *J. Am. Chem. Soc*., 2010, **132**, 3177–3186.

[51] E. Florez, T. Gomez, P. Liu, J.A. Rodriguez and F. Illas, *ChemCatChem*., 2010, **2**, 1219–1222.

[52] H. Prats, R.A. Gutiérrez, J.J. Piñero, F. Viñes, S.T. Bromley, P.J. Ramírez, J.A. Rodriguez and F. Illas, *J. Am. Chem. Soc*., 2019, **141**, 5303–5313.

[53] J.A. Rodriguez, P. Liu, D.J. Stacchiola, S.D. Senanayake, M.G. White and J.G. Chen, *ACS Catal*., 2015, **5**, 6696–6706.

[54] A.B. Vidal, L. Feria, J. Evans, Y. Takahashi, P. Liu, K. Nakamura, F. Illas and J.A. Rodriguez, *J. Phys. Chem. Lett*., 2012, **3**, 2275–2280.

[55] J.A. Rodriguez, J. Evans, L. Feria, A.B. Vidal, P. Liu, K. Nakamura and F. Illas, *J. Catal*., 2013, **307**, 162–169.

[56] J.A. Rodriguez, F. Viñes, F. Illas, P. Liu, Y. Takahashi and K. Nakamura, *J. Chem. Phys*., 2007, **127**, 211102-4.

[57] E. Florez, L. Feria, F. Viñes, J.A. Rodriguez and F. Illas, *J. Phys. Chem. C*., 2009, **113**, 19994–20001.

[58] S. Posada-Pérez, F. Viñes, J.A. Rodríguez and F. Illas, *J. Chem. Phys*., 2015, **143**, 114704-11.

[59] G. Kresse and J. Hafner, *Phys. Rev. B*., 1993, **47**, 558–561

[60] G. Kresse and J. Furthmüller, *Phys. Rev. B*., 1996, **54**, 11169–11186.

[61] G. Kresse and J. Furthmüller, *Comp. Mater. Sci.*, 1996, **6**, 15–50.

[62] G. Kresse and D. Joubert, *Phys. Rev. B*., 1999, **59**, 1758–1775.

[63] J. Wellendorff, K.T. Lundgaard, A. Møgelhøj, V. Petzold, D.D. Landis, J.K. Nørskov, T. Bligaard and K.W. Jacobsen, *Phys. Rev. B*., 2012, **85**, 235149-23.

[64] J. Wellendorff, T.L. Silbaugh, D. Garcia-Pintos, J.K. Nørskov, T. Bligaard, F. Studt and C.T. Campbell, *Surf. Sci.*, 2015, **640**, 36–44.

[65] C.T. Campbell, *Acc. Chem. Res*., 2019, **52**, 984–993.

[66] F. Viñes, C. Sousa, P. Liu, J.A. Rodriguez and F. Illas*, J. Chem. Phys*., 2005, **122**, 174709-11.

[67] H.J. Monkhorst and J.D. Pack, *Phys. Rev. B*., 1976, **13**, 5188–5192.

[68] A.S. Chaves, M.J. Piotrowski and J.L.F. Da Silva, *Phys. Chem. Chem. Phys*., 2017, **19**, 15484–15502.

[69] W. Song, W.-C. Lu, C.Z. Wang and K.M. Ho, *Comput. Theor. Chem.*, 2011, **978**, 41–46.

[70] M. Methfessel and A.T. Paxton, *Phys. Rev. B*., 1989, **40**, 3616–3621.

[71] K. Momma and F. Izumi, *J. Appl. Crystallogr*., 2011, 44, 1272–1276.

[72] Kittle, C. *Introduction to Solid State Physics*, 8th edition, Hoboken, NJ: John Wiley & Sons, Inc, 2005.

[73] P. Janthon, S. M. Kozlov, F. Viñes, J. Limtrakul, and F. Illas, *J. Chem. Theory Comput*., 2013, **9**, 1631-1640.

[74] P. Janthon, S. Luo, S. M. Kozlov, F. Viñes, J. Limtrakul, D. G. Truhlar and F. Illas, *J. Chem. Theory Comput*., 2014, **10**, 3832-3839.

[75] T. Gomez, E. Florez, J.A. Rodriguez and F. Illas, *J. Phys. Chem. C*., 2011, **115**, 11666–11672.

[76] R.F.W. Bader, *Chem. Rev*., 1991, **91**, 893–928.

[77] J. A. Rodriguez and F. Illas, *Phys. Chem. Chem. Phys*., 2012, **14**, 427-438.

Graphic abstract for TOC

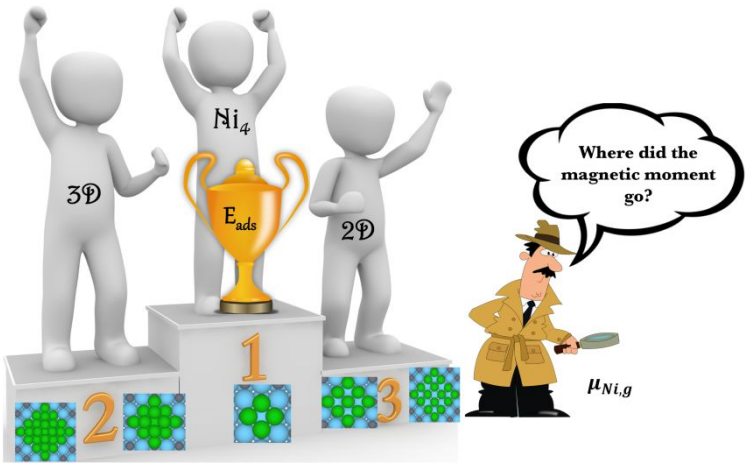

Ni clusters adsorb on TiC with a quenching in their magnetic moment